REPORT DOCUMENTATION PAGE

Form Approved OMB NO. 0704-0188

The public reporting burden for this collection of information is estimated to average 1 hour per response, including the time for reviewing instructions, searching existing data sources, gathering and maintaining the data needed, and completing and reviewing the collection of information. Send comments regarding this burden estimate or any other aspect of this collection of information, including suggesstions for reducing this burden, to Washington Headquarters Services, Directorate for Information Operations and Reports, 1215 Jefferson Davis Highway, Suite 1204, Arlington VA, 22202-4302. Respondents should be aware that notwithstanding any other provision of law, no person shall be subject to any oenalty for failing to comply with a collection of information if it does not display a currently valid OMB control number.
PLEASE DO NOT RETURN YOUR FORM TO THE ABOVE ADDRESS.

1. REPORT DATE (DD-MM-YYYY)	2. REPORT TYPE	3. DATES COVERED (From - To)
27-07-2012	Conference Proceeding	-

4. TITLE AND SUBTITLE
ImpactPoint Prediction for Thrusting Projectiles in the Presence of Wind

5a. CONTRACT NUMBER
W911NF-10-1-0369

5b. GRANT NUMBER

5c. PROGRAM ELEMENT NUMBER
611102

6. AUTHORS
Y. Bar-Shalom, P. K. Willett , D. Hardiman, T. Yuan

5d. PROJECT NUMBER

5e. TASK NUMBER

5f. WORK UNIT NUMBER

7. PERFORMING ORGANIZATION NAMES AND ADDRESSES
University of Connecticut - Storrs
Office for Sponsored Programs
University of Connecticut
Storrs, CT 06269 -1133

8. PERFORMING ORGANIZATION REPORT NUMBER

9. SPONSORING/MONITORING AGENCY NAME(S) AND ADDRESS(ES)
U.S. Army Research Office
P.O. Box 12211
Research Triangle Park, NC 27709-2211

10. SPONSOR/MONITOR'S ACRONYM(S)
ARO

11. SPONSOR/MONITOR'S REPORT NUMBER(S)
57823-CS.38

12. DISTRIBUTION AVAILIBILITY STATEMENT
Approved for public release; distribution is unlimited.

13. SUPPLEMENTARY NOTES
The views, opinions and/or findings contained in this report are those of the author(s) and should not contrued as an official Department of the Army position, policy or decision, unless so designated by other documentation.

14. ABSTRACT
In estimating the state of thrusting/ballistic endoatmospheric projectiles for the end purpose of impact point prediction (IPP), the total observation time, the wind effect and the sensor accuracy significantly affect the IPP performance. First the tracker accounting for the wind effect is presented. Following this, based on the multiple interacting multiple model (MIMM) estimator developed recently, a sensitivity study of the IPP performance with respect to the total observation time, the wind (strength and direction) and the sensor accuracy is presented.

15. SUBJECT TERMS
ImpactPoint Prediction, Wind

16. SECURITY CLASSIFICATION OF:			17. LIMITATION OF ABSTRACT	15. NUMBER OF PAGES	19a. NAME OF RESPONSIBLE PERSON
a. REPORT	b. ABSTRACT	c. THIS PAGE			Yaakov Bar-Shalom
UU	UU	UU	UU		19b. TELEPHONE NUMBER 860-486-4823

Report Title

ImpactPoint Prediction for Thrusting Projectiles in the Presence of Wind

ABSTRACT

In estimating the state of thrusting/ballistic endoatmospheric projectiles for the end purpose of impact point prediction (IPP), the total observation time, the wind effect and the sensor accuracy significantly affect the IPP performance. First the tracker accounting for the wind effect is presented. Following this, based on the multiple interacting multiple model (MIMM) estimator developed recently, a sensitivity study of the IPP performance with respect to the total observation time, the wind (strength and direction) and the sensor accuracy is presented.

Conference Name: SPIE Conf. Signal Processing, Sensor Fusion, and Target Recognition XXI

Conference Date: April 16, 2012

Impact Point Prediction for Thrusting Projectiles in the Presence of Wind

Ting Yuan[a], Yaakov Bar-Shalom[a], Peter Willett[a] and David Hardiman[b]

[a] University of Connecticut, Storrs CT
[b] AMRDEC, Huntsville AL

ABSTRACT

In estimating the state of thrusting/ballistic endoatmospheric projectiles for the end purpose of impact point prediction (IPP), the total observation time, the wind effect and the sensor accuracy significantly affect the IPP performance. First the tracker accounting for the wind effect is presented. Following this, based on the multiple interacting multiple model (MIMM) estimator developed recently, a sensitivity study of the IPP performance with respect to the total observation time, the wind (strength and direction) and the sensor accuracy is presented.

Keywords: multiple interacting multiple model estimators, extended Kalman filter, impact point prediction, sensitivity, wind effect

1. INTRODUCTION

The impact point prediction (IPP) of a thrusting/ballistic projectile is affected by the following important practical issues: the total observation time, the wind effect and the sensor accuracy.

The very short total observation time is one of the major challenges we always face in practical situations. For the IPP problem, using a state model with drag coefficient and thrust estimated as separate components, it is very important to have enough available total observation time to initialize the estimator, overcome the estimation ambiguity between the drag coefficient and the thrust and have the probability of the correct mode converge close to unity before the prediction procedure starts [10]. The available observation time is thus one of the key factors that significantly affect the IPP performance. To achieve a desired IPP performance using only the observation data collected in a very limited time necessitates a sensitivity study of the IPP performance with respect to the total observation time.

The wind, as one of the important meteorological parameters for endoatmospheric projectiles, can significantly affect the IPP performance. The wind effect causes the moving projectile to turn into the "apparent" wind, i.e., causes the nose of the moving projectile to be pointed into the wind [13]. We shall assume a constant wind during the estimation and prediction procedure.[1] A tail or head wind, if unaccounted for, would cause the IPP to give under- or over-prediction for the projectile's range, hence the term range wind effect; a cross wind would lead to left- or right-deviation. The vertical wind is ignored in this study, as it is typically not significant. Consequently, the projectile's dynamic model is modified from [9, 10] to incorporate the wind effect and, based on the modified model, the sensitivity of the IPP performance with respect to the wind strength and direction is studied.

The sensor accuracy also has a significant impact on the IPP performance. Due to the nonlinear nature of the dynamics of the thrusting/ballistic projectiles, linearization and discretization of the nonlinear system is an approximation of reality. For a fixed sampling rate, the approximation quality is determined by the sensor accuracy. The observation uncertainty caused by the sensor errors in range and in angles (azimuth and elevation) affects the estimation result, as well as the prediction procedure that follows, and hence the final IPP performance.

[0]Proc. SPIE Conference Signal Processing, Sensor Fusion, and Target Recognition XXI, # 8392-63, Baltimore MD, April 2012. Research sponsored by ARO W911NF-10-1-0369 and ONR N00014-10-1-0029.

[1]The wind is considered as a constant during the whole trajectory period. Altitude and location-dependent wind could also be considered.

In this paper, based on the multiple interacting multiple model (MIMM) estimator (with different initial drag coefficient estimates and using unbiased mixing) developed earlier in [10], the sensitivity of the IPP performance with respect to the total observation time, the wind effect and the sensor accuracy are extensively studied.

The paper is organized in the following manner. Under a flat Earth assumption (suitable for short range projectiles), the dynamic model with its corresponding discretized form and the measurement model are presented in Section 2. The wind effect and the corresponding modified dynamic model are presented in Section 3. The MIMM estimator and the IPP procedure are described in Section 4. The parameter selection for the design of the MIMM estimator and an N-point adaptive initialization approach are presented in Section 5. Then the sensitivity of the IPP performance with respect to the total observation time, the wind effect and the sensor accuracy is evaluated by simulation in Section 6. Conclusions are presented in Section 7.

2. DYNAMIC MODEL AND MEASUREMENT MODEL

The trajectory of a thrusting projectile, from launch to impact, can be divided into two phases: thrusting and ballistic. An IMM estimator with a thrust mode (TM) and a ballistic mode (BM) to match these phases is the natural choice.

The state vector for the TM is denoted as

$$\mathbf{x}(t) = [\, x(t) \;\; y(t) \;\; z(t) \;\; \dot{x}(t) \;\; \dot{y}(t) \;\; \dot{z}(t) \;\; \alpha(t) \;\; \tau(t) \,]' \tag{1}$$

where $\alpha(t)$ is the drag coefficient and $\tau(t)$ is the thrust. The state vector of the BM is the same as above but excludes the thrust component. The time arguments will be omitted where no ambiguity is casued.

It is known that the drag coefficient varies significantly with the Mach number regime: subsonic, transonic and supersonic. This will be accounted for by a Mach number-dependent multiplier.

Under flat Earth assumption, the dynamic model for this problem can be written as follows

$$\begin{bmatrix} \ddot{x} \\ \ddot{y} \\ \ddot{z} \end{bmatrix} = \frac{\tau}{V} \begin{bmatrix} \dot{x} \\ \dot{y} \\ \dot{z} \end{bmatrix} + \alpha\, \alpha_m\, D \begin{bmatrix} \dot{x} \\ \dot{y} \\ \dot{z} \end{bmatrix} + g \begin{bmatrix} 0 \\ 0 \\ -1 \end{bmatrix} + \tilde{\nu}_1 \tag{2}$$

and

$$\dot{\alpha} = \tilde{\nu}_2 \tag{3}$$

$$\dot{\tau} = \tilde{\nu}_3 \tag{4}$$

where

- The first term on the right side of (2) is the specific thrust in the x, y, and z directions. For the ballistic phase, the thrust is zero.
- The second term is the drag part, which is related to velocity and altitude.
- V is the magnitude of the velocity $\mathbf{v} = [\, \dot{x} \;\; \dot{y} \;\; \dot{z} \,]'$, i.e., the speed (in m/ s).
- α is the drag coefficient (in m^2/kg) at subsonic speed and τ is the thrust (in m^2/s).
- α_m is the (dimensionless) *Mach number-dependent drag coefficient multiplier*, which is approximated by a cubic spline curve shown in [10] (based on the curve with sharp nose projectile in [12]).
- $D = -\frac{\rho(z)V}{2}$, where $\rho(z) = \rho_0 e^{-cz}$ is the air density (in $\mathrm{kg/m}^3$) at altitude z (in m) and c is the air density constant (in m^{-1}) [8].
- g is the standard acceleration due to gravity at sea level, assumed to be the same throughout the trajectory, with value 9.812 $\mathrm{m/s}^2$.
- $\tilde{\nu}_1$, $\tilde{\nu}_2$, and $\tilde{\nu}_3$ are assumed to be continuous-time zero-mean white Gaussian noises. The drag coefficient and thrust acceleration are thus modeled as Wiener processes with slow variation [1].

Combining the dynamic equations (2)–(4), we have the following compact form

$$\dot{\mathbf{x}}(t) = f[\mathbf{x}(t)] + \tilde{\nu}(t) \tag{5}$$

where

$$f[\mathbf{x}(t)] = \begin{bmatrix} \dot{x}(t) \\ \dot{y}(t) \\ \dot{z}(t) \\ \tau\dfrac{\dot{x}(t)}{V(t)} + \alpha(t)\alpha_m(t)D(t)\dot{x}(t) \\ \tau(t)\dfrac{\dot{y}(t)}{V(t)} + \alpha(t)\alpha_m(t)D(t)\dot{y}(t) \\ \tau(t)\dfrac{\dot{z}(t)}{V(t)} + \alpha(t)\alpha_m(t)D(t)\dot{z}(t) - g \\ 0 \\ 0 \end{bmatrix} \tag{6}$$

and

$$\tilde{\nu}(t) = [\, \tilde{\nu}_1(t)' \;\; \tilde{\nu}_2(t) \;\; \tilde{\nu}_3(t) \,]' \tag{7}$$

Note that $\alpha_m(t)$ is March-number dependent and $D(t)$ is assumed to be related to both altitude and velocity.

Using the discrete time notation $\mathbf{x}(k) = \mathbf{x}(t)|_{t=kT}$ and $\mathbf{x}(k+1) = \mathbf{x}(t+T)|_{t=kT}$, we have the discretized form for (5) by a second order Taylor expansion [4] as

$$\mathbf{x}(k+1) = \mathbf{x}(k) + f[\mathbf{x}(k)]T + A(k)f[\mathbf{x}(k)]\frac{T^2}{2} + \nu(k) \tag{8}$$

where $A(k)$ is the Jacobian of (6) evaluated at $\mathbf{x}(k)$ and $\nu(k)$ is the discretized continuous time process noise for the sampling interval T. Based on the assumption that α is nearly constant and D is related to both z and V, the detailed form of A is given in [10].

The covariance matrix of the discretized process noise is

$$Q = \begin{bmatrix} \begin{bmatrix} \frac{T^3}{3}I_3 & \frac{T^2}{2}I_3 \\ \frac{T^2}{2}I_3 & TI_3 \end{bmatrix} q_v & \mathbf{0}_{6\times 1} & \mathbf{0}_{6\times 1} \\ \mathbf{0}_{1\times 6} & Tq_\alpha & 0 \\ \mathbf{0}_{1\times 6} & 0 & Tq_\tau \end{bmatrix} \tag{9}$$

where I_3 is the 3×3 identity matrix and the continuous time process noise "intensities" q_v, q_α and q_τ are the corresponding power spectral densities (PSD).

Assuming the sensor is located at $(\, x_s \;\; y_s \;\; z_s \,)$, the measurements in spherical coordinates are

$$r_m = r + w_r = \sqrt{(x-x_s)^2 + (y-y_s)^2 + (z-z_s)^2} + w_r \tag{10}$$

$$\theta_m = \theta + w_\theta = \tan^{-1}\left(\frac{y-y_s}{x-x_s}\right) + w_\theta \tag{11}$$

$$\epsilon_m = \epsilon + w_\epsilon = \tan^{-1}\left(\frac{z-z_s}{\sqrt{(x-x_s)^2 + (y-y_s)^2 + (z-z_s)^2}}\right) + w_\epsilon \tag{12}$$

where r, θ and ϵ are the independent true range, azimuth and elevation components, respectively. w_r, w_θ and w_ϵ denote the corresponding zero-mean white Gaussian measurement noises with standard deviations (SD) σ_r, σ_θ and σ_ϵ, respectively.

An unbiased measurement conversion from spherical to Cartesian coordinates was presented [2], so that the measurement can be described entirely in Cartesian coordinates as

$$\mathbf{z}(k) \triangleq H\mathbf{x}(k) + \mathbf{w}(k) \tag{13}$$

where $H = [\, I_3 \;\; \mathbf{0} \,]$, $\mathbf{w}(k)$ is the equivalent measurement noise vector in Cartesian coordinates obtained from the unbiased measurement conversion and $R(k)$ is the corresponding equivalent *state-dependent* covariance matrix.

3. WIND EFFECT

To estimate the state of thrusting/ballistic endoatmospheric projectiles one has to model the wind effect, which is one of the important meteorological factors that can significantly affect the IPP performance in many practical situations.

The contribution of the wind comprises the range wind, cross wind and vertical wind effects. The vertical wind is generally considered as less important and is ignored in the present study. The range (head/tail) wind will pull back or push forward the moving object and the cross wind causes the moving object deviate to the side. These wind components together comprise the true wind velocity and are combined with the target velocity (with respect to the ground) to yield the so-called "apparent wind". The moving target turns into the apparent wind, i.e., its nose is pointed into the wind (or "upwind") while its tail pointing "downwind" [13]. With the wind effect shown in Fig. 1, we have

$$\mathbf{v}_a = \mathbf{v}_w - \mathbf{v} \tag{14}$$

where $\mathbf{v}$ is the target ground velocity, $\mathbf{v}_w$ is the wind velocity and $\mathbf{v}_a$ is the apparent wind velocity.

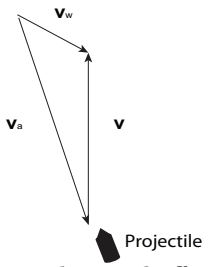

Figure 1: The wind effect.

Assuming the wind is constant and as the drag and the thrust in the dynamic model should be aligned with the direction of the projectile, which is aligned with the apparent wind, we have the modified version (accounting for the wind effect) of the dynamic model described in (2) as follows

$$\begin{bmatrix} \ddot{x} \\ \ddot{y} \\ \ddot{z} \end{bmatrix} = \frac{\tau}{V_a} \begin{bmatrix} \dot{x} - \dot{x}_w \\ \dot{y} - \dot{y}_w \\ \dot{z} - \dot{z}_w \end{bmatrix} + \alpha\, \alpha_m\, D_a \begin{bmatrix} \dot{x} - \dot{x}_w \\ \dot{y} - \dot{y}_w \\ \dot{z} - \dot{z}_w \end{bmatrix} + g \begin{bmatrix} 0 \\ 0 \\ -1 \end{bmatrix} + \tilde{\nu}_1 \tag{15}$$

where, as in (2), τ is the thrust, α is the drag coefficient, α_m is the (dimensionless) Mach number-dependent drag coefficient multiplier and g is the standard gravity. In addition, we have the apparent wind magnitude V_a, the true wind components $\dot{x}_w$, $\dot{y}_w$ and $\dot{z}_w$ in Cartesian coordinates and the new drag coefficient factor $D_a = -\frac{\rho(z)V_a}{2}$. The process noise $\tilde{\nu}_1$ is assumed to be zero mean white Gaussian, the same as in (2). A sample scenario with the cross or/and range (tail) wind is illustrated in Fig. 2 (the trajectories of the projectile of caliber 120 mm with no wind present, "W0"; 10 m/s cross wind, "C10"; 7 m/s cross wind and 7 m/s tail wind, "C7T7").

Accordingly, the modified version of the dynamic equation (5) is

$$\dot{\mathbf{x}}(t) = f_w[\mathbf{x}(t),\ \mathbf{x}_w(t)] + \tilde{\nu}(t) \tag{16}$$

where

$$f_w[\mathbf{x}(t),\ \mathbf{x}_w(t)] = \begin{bmatrix} \dot{x}(t) \\ \dot{y}(t) \\ \dot{z}(t) \\ \tau\dfrac{\dot{x}(t) - \dot{x}_w(t)}{V_a(t)} + \alpha(t)\alpha_m(t)D_a(t)[\dot{x}(t) - \dot{x}_w(t)] \\ \tau\dfrac{\dot{y}(t) - \dot{y}_w(t)}{V_a(t)} + \alpha(t)\alpha_m(t)D_a(t)[\dot{y}(t) - \dot{y}_w(t)] \\ \tau\dfrac{\dot{z}(t) - \dot{z}_w(t)}{V_a(t)} + \alpha(t)\alpha_m(t)D_a(t)[\dot{z}(t) - \dot{z}_w(t)] - g \\ 0 \\ 0 \end{bmatrix} \tag{17}$$

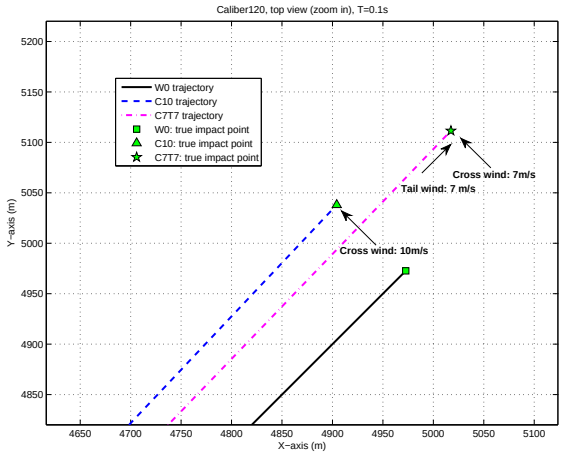

Figure 2: A sample scenario illustrating the wind effect.

with the wind effect compensation vector

$$\mathbf{x}_w(t) = [\,0 \;\; 0 \;\; 0 \;\; \dot{x}_w(t) \;\; \dot{y}_w(t) \;\; \dot{z}_w(t) \;\; 0 \;\; 0\,]' \tag{18}$$

and $\tilde{\nu}(t)$ is as in (7).

The discretized form of the modified dynamic equation (17) and its Jacobian are modified accordingly.

4. MULTIPLE IMM ESTIMATOR FOR IPP

In the TM, the drag parameter (drag coefficient) and thrust are separate state components as shown in (1). However, the drag force and thrust force are acting simultaneously (see equation (2)) and the IMM estimator has difficulty distinguishing between them if the initial uncertainty in the drag coefficient is large. The sensitivity of the estimation to the initial drag coefficient estimate necessitates the use of an MIMM estimator to overcome this "marginal observability" problem [1].

The procedure starts by establishing a set of L IMM estimators, each with an appropriate set of modes (TM and BM in present case) to describe the system behavior. Each IMM estimator will be initialized with a different value of the drag coefficient with a suitable initial standard deviation (SD). The initial SD is taken equal to 25% of the initial estimate of the drag coefficient. The filter design parameters are discussed in Section 5.

In order to select the best initial drag coefficient estimate, we need to determine the most likely one of the L IMM estimators, during the observation period. The likelihood function of IMM estimator l for the time interval $[k_0,\, K]$ is

$$\Lambda_l^{k_0,K} = \prod_{k=k_0}^{K} \Lambda_l\,(k) \qquad\qquad l = 1, \ldots,\, L \tag{19}$$

where [2]

$$\Lambda_l(k) = \sum_{j=1}^{r} \left\{ \mathcal{N}\left[\mathbf{z}(k); \hat{\mathbf{z}}_l^i(k|k-1), S_l^i(k)\right] \sum_{j=1}^{r} p_{ji}\mu_l^j(k-1) \right\} \tag{20}$$

with $\mathcal{N}[\,\cdot\,]$ is the Gaussian probability density function, $\hat{\mathbf{z}}_l^i$ is the predicted measurement, S_l^i is the innovation covariance in mode i of IMM estimator l, $\mu_l^j(k-1)$ is the mode probability of mode j of IMM estimator l at time $k-1$ and p_{ji} is the transition probability from mode j to mode i over one sampling time interval. Then

$$l^* = \arg\max_l \Lambda_l^{k_0,K} = \arg\min_l \left[-\ln \Lambda_l^{k_0,K}\right] \tag{21}$$

selects the *best IMM estimator*. This yields the best initial estimate of the drag coefficient.

Based on the MIMM estimator, we can choose at the end of the observation period the most likely initial drag coefficient from the most probable mode from the best IMM estimator (21)[2]. Then a numerical IPP algorithm (we use the 4th order Runge-Kutta method [7], incorporating the wind effect if the wind information is available) is employed to predict the trajectory down to its impact point (at a known altitude, assumed here to be zero). At the same time, the corresponding covariance is also predicted to the impact point using a zero-gain (open loop) EKF covariance equation. Then the 99% chi-square probability region ellipse for the true impact point is [1]

$$[\, x_{ip} - \hat{x}_{pd} \;\; y_{ip} - \hat{y}_{pd} \,]\, P_{pd}^{-1} \begin{bmatrix} x_{ip} - \hat{x}_{pd} \\ x_{ip} - \hat{y}_{pd} \end{bmatrix} = \chi_2^2\,(99\%) \tag{22}$$

where $(x_{ip} \;\; y_{ip})$ is the true impact point, $(\hat{x}_{pd} \;\; \hat{y}_{pd})$ is the predicted impact point, P_{pd} is the corresponding predicted covariance matrix, and $\chi_2^2\,(99\%)$ denotes the 99% point on the chi-square cumulative distribution function with two degrees of freedom [1]. This can be used as the "warning zone" in practical situations.

5. MIMM PARAMETER SETTING

The MIMM estimator using unbiased mixing with different initial drag coefficient estimates is used [10]. The unbiased mixing is necessary because of the different dimension state vectors in the two modes (TM and BM).

The MIMM estimator is chosen to consist of $L = 4$ IMM estimators with initial drag coefficient estimates $\hat{\alpha}^i(0),\;\; i = 1, 2, 3, 4$ as 0.18, 0.13, 0.065 and 0.03 (m^2/kg), respectively.[3] The initial SD of each drag coefficient estimate is 25% of the corresponding initial estimate of the drag coefficient.

In the dynamic equations, we actually assume a nearly constant velocity model (continuous time white noise acceleration — CWNA [1]) for the kinematic components and a Wiener process with slow variation for the drag coefficient and thrust. In order to satisfy this model's assumptions, we choose small process noise "intensities" (power spectral densities — PSD) based on the process noise induced RMS change (in velocity d_v/ drag coefficient d_α/ thrust d_τ) over an interval of 1 s [10], as shown in Table 1. Note that d_v is chosen differently for the four initial drag coefficient estimates $\hat{\alpha}^i(0),\;\; i = 1, 2, 3, 4$.

Table 1: The RMS change rates due to the process noise

Filter	d_v [(m/s)/s]				d_α [(m^2/kg)/s]	d_τ [(m/s^2)/s]
	$\hat{\alpha}^1(0)$	$\hat{\alpha}^2(0)$	$\hat{\alpha}^3(0)$	$\hat{\alpha}^4(0)$		
IMM (TM)	3.5	2.5	2	1	$0.12\hat{\alpha}^i(0)$/s	$0.25\,\hat{\tau}(0)$/s
IMM (BM)	1.6	1.4	1.2	0.9	$0.10\hat{\alpha}^i(0)$/s	N/A

The transition probability matrix for the two-mode IMM is chosen based on the mean sojourn time [1] as

$$\pi = \begin{bmatrix} 0.950 & 0.050 \\ 0.002 & 0.998 \end{bmatrix} \tag{23}$$

with initial mode probability vector $[\,0.90 \;\; 0.10\,]$ for TM and BM.

The initialization is crucial to the accuracy of the state estimates. Due to the high sensitivity of the estimation with respect to the drag coefficient, which is velocity (Mach number)-dependent and "marginally distinguishable" from the thrust estimate, an N-point adaptive initialization method is used here (the number N is discussed later). This method is based on the polynomial fitting of a set of noisy position measurements [1], with the polynomial order adaptively chosen based on the corresponding goodness-of-fit error.

[2]In practice, the thrusting period is relatively short and by the end of the observation period the BM should be the dominant one in the IMM. Otherwise, if one does not know the burnout time (which is typically the case), one cannot make a meaningful IPP.

[3]This grid of values was chosen based on the tracking results in the absence of wind. It seems that the 60 mm projectile has a somewhat different drag coefficient in the presence of wind (it turns somewhat slowly into the wind). In the absence of information about how fast the projectiles align themselves with the apparent wind, it is assumed that this happens instantaneously.

The N-point fitting of a polynomial of order n is done as follows. The position measurements for the three Cartesian coordinates are

$$\begin{aligned} \mathbf{z}(k) &= H_{\mathbf{a}}(k)\mathbf{a} + w(k) \\ &\triangleq \begin{bmatrix} \mathbf{h}(k)' & \mathbf{0} & \mathbf{0} \\ \mathbf{0} & \mathbf{h}(k)' & \mathbf{0} \\ \mathbf{0} & \mathbf{0} & \mathbf{h}(k)' \end{bmatrix} \begin{bmatrix} \mathbf{a}_x \\ \mathbf{a}_y \\ \mathbf{a}_z \end{bmatrix} + w(k) \end{aligned} \tag{24}$$

where $k = 1, 2, \ldots, N$ and

$$\mathbf{h}(k) = \begin{bmatrix} 1 & t_k & \cdots & \dfrac{(t_k)^n}{n!} \end{bmatrix}' \tag{25}$$

with t_k is the sampling time and the parameter vectors

$$\mathbf{a}_i = [\, a_{i0} \;\; a_{i1} \;\; \cdots \;\; a_{in} \,]' \qquad\qquad i = x,\; y,\; z \tag{26}$$

contain the coefficients of the polynomials (one for each coordinate).

For the time covered by N points, we get the estimate for the parameter vector $\mathbf{a}$ (of dimension $3(n+1)$) as

$$\hat{\mathbf{a}} = \left[H_{\mathbf{a}}^{N'} \left(R^N\right)^{-1} H_{\mathbf{a}}^{N} \right]^{-1} H_{\mathbf{a}}^{N'} \left(R^N\right)^{-1} \mathbf{z}^N \tag{27}$$

with the corresponding covariance matrix

$$P_{\mathbf{a}} = \left[H_{\mathbf{a}}^{N'} \left(R^N\right)^{-1} H_{\mathbf{a}}^{N} \right]^{-1} \tag{28}$$

where, for the fitting interval, the stacked vector of measurements (of dimension $3N \times 1$), the stacked measurement matrix (of dimension $3N \times 3(n+1)$) and the block diagonal covariance matrix of measurement noise (of dimension $3N \times 3N$) are

$$\mathbf{z}^N = \begin{bmatrix} \mathbf{z}(1) \\ \vdots \\ \mathbf{z}(N) \end{bmatrix} \qquad H_{\mathbf{a}}^N = \begin{bmatrix} H_{\mathbf{a}}(1) \\ \vdots \\ H_{\mathbf{a}}(N) \end{bmatrix} \qquad R^N = \begin{bmatrix} R(1) & \cdots & \mathbf{0} \\ \vdots & \ddots & \vdots \\ \mathbf{0} & \cdots & R(N) \end{bmatrix} \tag{29}$$

respectively.

The goodness-of-fit error has the following chi-square distribution [1]

$$J_N \triangleq \left[\mathbf{z}^N - H_{\mathbf{a}}^N \hat{\mathbf{a}}\right]' \left(R^N\right)^{-1} \left[\mathbf{z}^N - H_{\mathbf{a}}^N \hat{\mathbf{a}}\right] \sim \chi^2_{3N-n_{\mathbf{a}}} \tag{30}$$

Using as acceptance region for (30) its 99% probability region, we can adaptively choose the best order n^*. This is done by starting with $n = 1$ and increasing it until the test statistic (30) falls below the 99% probability threshold. Based on the selected order, we obtain the estimate $\mathbf{a}^*$ (of dimension $3(n^*+1)$) and the corresponding covariance matrix $P_{\mathbf{a}}^*$. This is used to initialize the position, velocity and thrust components in the state vector $\mathbf{x}$.

The N-point adaptive initialization used $N = 12$ (about 1 s data). The constant velocity (CV, $n^* = 1$) and the constant acceleration (CA, $n^* = 2$) may be selected in the present study. Typically, $n^* = 2$, in which case the acceleration estimate is used (after subtracting the gravity acceleration and drag vector) to obtain the initial estimate of the thrust, $\hat{\tau}(0)$. If the model choice is $n^* = 1$ (this happens rarely, for a low thrust projectile), then $\hat{\tau}(0) = g$ with SD $g/4$.

6. SIMULATION RESULTS

Three categories of thrusting/ballistic projectiles of different caliber sizes are considered: 60 mm, 81 mm and 120 mm. For each category, there are trajectories with no wind present, labeled as "W0"; with 5 m/s cross wind only, labeled as "C5"; with 10 m/s cross wind only, labeled as "C10"; with 5 m/s cross wind and 5 m/s tail wind, labeled as "C5T5"; with 7 m/s cross wind and 7 m/s tail wind, labeled as "C7T7". Note that the tail wind blows in the travel direction of the projectiles [13]. Totally, 15 trajectories were generated using [11] with flat Earth model with quadrant elevation 45° (i.e., aimpoint is NE). Measurements were obtained with no missed detections and no false alarms.

The parameters of the trajectories of the different caliber projectiles considered, namely, the projectile range to impact (R^t), the impact time (T^t_{ip}), the sampling interval (T), the maximum ground speed (V^t_{max}), the ground speed at impact point (V^t_{ip}) and the apogee altitude (H^t_{apg}), are summarized in Table 2. The launch point of each projectile was at the origin of coordinates. The sensor location was (5000 4000 0) m.

As shown in Table 3, four different sensor accuracy settings are used and labeled as *Case* 1 (good sensor accuracy), *Case* 2 (bad angle accuracy), *Case* 3 (bad range accuracy) and *Case* 4 (excellent sensor accuracy).

Table 2: The parameters of the trajectories of the different caliber projectiles considered

Caliber	R^t (m)	T^t_{ip} (s)	T (s)	V^t_{max} (m /s)	V^t_{ip} (m /s)	H^t_{apg} (m)
60 mm	3600 ± 100	30 ± 1	0.1	240 ± 3	155 ± 3	1085 ± 5
81 mm	5700 ± 100	37 ± 1	0.1	295 ± 3	200 ± 3	1680 ± 10
120 mm	7150 ± 150	41 ± 1	0.1	315 ± 5	230 ± 5	2055 ± 10

Table 3: Sensor accuracy settings

	σ_r	σ_θ	σ_ϵ
Case 1	10 m	5 mrad	5 mrad
Case 2	10 m	10 mrad	10 mrad
Case 3	25 m	5 mrad	5 mrad
Case 4	5 m	3 mrad	3 mrad

With 100 Monte Carlo (MC) runs for each sensor accuracy, we examine the IPP performance with "given wind information" (g.w.i.) and with "no wind information" provided (n.w.i.) for different *total observation time percentages of the whole trajectory* (denoted as "OT" for conciseness): 15%, 20%, 25%, 30%, 40% and 50%. Particularly, under the same sensor accuracy and the same OT setting, in each MC run, the same random number set (but different in different MC runs, of course) has been used for different trajectories (W0/ C5/ C10/ C5T5/ C7T7) to examine how significant the wind effect affects the IPP performance with the corresponding wind information provided.

Note that all the IPP results are *by default* obtained with given wind information unless "n.w.i" is indicated. The indicating term "g.w.i." is omitted in Figures, Tables and discussions if there is no ambiguity.

A sample estimated trajectory, indicating the portions corresponding to the MIMM filtering and to the IPP, including the estimated burnout point (BoP) and the uncertainty ellipse centered at the true impact point, is presented in Fig. 3.

6.1 IPP RMS Error

The IPP root mean square (RMS) errors of the trajectories of caliber 60 mm, 81 mm and 120 mm (in different situations) are shown in Tables 4, 5 and 6, respectively. The IPP RMS errors (g.w.i. and n.w.i.) for different OTs and different sensor accuracies are evaluated and compared.

From Tables 4–6, it can be seen that, generally, as the wind becomes stronger, the difference between the IPP RMS error (g.w.i.) and the IPP RMS error (n.w.i.) will increase, especially for smaller OTs; as OT increases, the influence of the wind on the IPP performance becomes smaller. As the sensor accuracy becomes worse, the IPP performance is gradually degraded. Particularly, the sensor error that causes more uncertainty along the travel direction of the projectiles, compared with the sensor error that causes more uncertainty perpendicular to

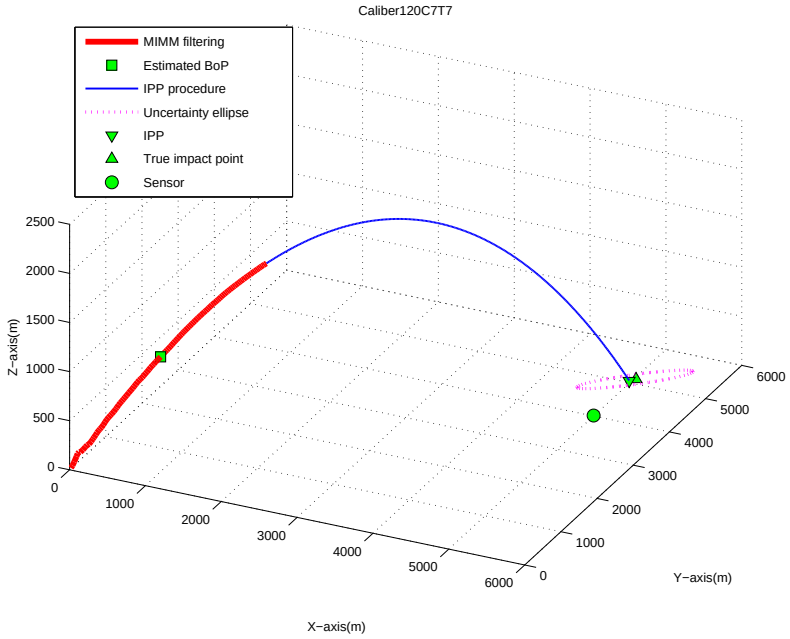

Figure 3: A sample estimated trajectory with IPP uncertainty ellipse centered at true impact point.

travel direction of the projectiles, has more influence on the IPP performance. We can get an IPP RMS error up to 507.9 m (Table 4: *Case* 2, OT=15% and 60C7T7 (n.w.i.)) for 60 mm, 708.5 m (Table 5: *Case* 3, OT=15% and 81C7T7 (n.w.i.)) for 81 mm and 948.4 m (Table 6: *Case* 3, OT=15% and 120C7T7 (n.w.i.)) for 120 mm. These are unacceptable errors of about 14%, 12% and 13% of the projectile ranges for 60 mm, 81 mm and 120 mm, respectively.[4] A strong wind effect, combined with a poor sensor accuracy, will lead to an unacceptable IPP RMS error when only a very short total observation time is available. If we have an excellent sensor accuracy in the presence of decent wind environment (Tables 4–6: *Case* 4), a good IPP performance always yields.

In Tables 4–6, the columns with the wind information provided (g.w.i.) show that, given a sufficient observation time (say, OT= 25%–50%) to correctly select the best IMM from the MIMM estimator, the IPP RMS errors are practically the same as without wind. This implies that the wind effect can be fully compensated if the wind information is correctly provided.

6.2 IPP Uncertainty Ellipse

With different OTs and sensor accuracies, the IPP uncertainty ellipses using (22), centered at the true impact point, with the corresponding *MC IPP "cloud of points"* (both g.w.i. and n.w.i.) for different caliber size trajectories in the presence of wind are shown in Figs. 4–6.

From Fig. 4, it can be seen that as the OT increases, more IPP points fall in the corresponding uncertainty ellipses and the size of the uncertainly eclipses gradually shrinks. The total observation time is crucial for the evaluation: given the OT is large enough (50%), most of the MC IPP points fall within the uncertainty ellipses with acceptable IPP RMS errors. The outliers are due to the forced early decision when OT is small.

From Fig. 5, it can be seen that as the sensor accuracy worsens, the corresponding IPP uncertainty ellipses are longer and fewer MC IPP points fall into them. Particularly, the larger sensor error in range (which causes more uncertainty along the major axis of uncertainty ellipse) results in the MC IPP points scattered more randomly along the major axis of the corresponding IPP uncertainty ellipse.

From Fig. 6, comparing the IPP clouds (n.w.i.) with smaller wind ("C5"/ "C5T5") to those (n.w.i.) with stronger wind ("C10"/"C7T7"), respectively, it is obvious that the stronger the wind is, the more significant the

[4]In practical situations, a minimum acceptable IPP RMS error is expected to be within 10% of the projectile range.

Table 4: IPP RMS errors (in m, 100 MC runs) for different OTs and different sensor accuracies, caliber 60 mm

Case 1	60W0	60C5	60C5(n.w.i.)	60C10	60C10(n.w.i.)	60C5T5	60C5T5(n.w.i.)	60C7T7	60C7T7(n.w.i.)
15%	520.6	520.1	518.6	520.1	520.6	508	501.1	484.4	500.1
20%	161.9	163.3	163.5	164.8	169.2	166.1	166.9	165.4	176.4
25%	134.5	135.2	136.4	136.1	147.9	134	154.7	134.2	164.1
30%	104.4	104	104.9	103.6	115.8	102.1	116	98.6	122.2
40%	61.2	61.1	66.8	60.9	79.5	59.2	73.5	58.4	81.3
50%	43.3	43.2	48.3	43.1	59.3	43.1	53.9	43.4	60.2
Case 2	60W0	60C5	60C5(n.w.i.)	60C10	60C10(n.w.i.)	60C5T5	60C5T5(n.w.i.)	60C7T7	60C7T7(n.w.i.)
15%	531.5	531	522.3	525.8	519.7	513.1	517.5	507.8	507.9
20%	213.6	213.5	210.1	213.4	211.9	220.2	220.3	220	225.1
25%	151.9	151.6	150.9	151.3	156.1	154.3	172.9	155.4	176.5
30%	117.4	116.7	116.7	116.1	122.1	120	132.5	121.1	139.1
40%	70.8	70.4	73.8	70.1	84.9	72.2	85.4	72.5	94.3
50%	54.3	54.1	58.6	53.9	69.2	56	65.2	56.7	71.7
Case 3	60W0	60C5	60C5(n.w.i.)	60C10	60C10(n.w.i.)	60C5T5	60C5T5(n.w.i.)	60C7T7	60C7T7(n.w.i.)
15%	369.8	372.3	367	378.9	369.2	368.4	385.6	368.4	385.1
20%	273.3	279.9	273.9	277	280.1	275.3	306.4	271.5	309.8
25%	197.2	187.7	200.7	188	210.8	197.5	209	195.8	217.5
30%	131.4	133.6	134.9	136.8	145.5	135.7	151.6	130.4	163.7
40%	104.6	105.4	108.3	104.9	115.3	98.3	105.8	92.7	109.8
50%	46	47.1	50.8	48.8	60.6	45.9	54.7	46.3	60.1
Case 4	60W0	60C5	60C5(n.w.i.)	60C10	60C10(n.w.i.)	60C5T5	60C5T5(n.w.i.)	60C7T7	60C7T7(n.w.i.)
15%	226.5	226.2	222.1	223	232.4	242.7	265.5	238.9	279.8
20%	138	137.5	141	137.2	153.9	133.1	153.7	133.8	160.6
25%	96.6	96.2	101.8	96.3	117.2	97.3	116.7	100.1	127.1
30%	75.4	75.1	82.4	75	97.7	76.3	87.8	74.2	94.7
40%	47.3	47.1	54	47.3	68.5	49	61.9	49.3	69.1
50%	35	35	40	35.1	50.3	35.1	45.2	35.4	51.2

Table 5: IPP RMS errors (in m, 100 MC runs) for different OTs and different sensor accuracies, caliber 81 mm

Case 1	81W0	81C5	81C5(n.w.i.)	81C10	81C10(n.w.i.)	81C5T5	81C5T5(n.w.i.)	81C7T7	81C7T7(n.w.i.)
15%	464.3	470.5	448.2	470.3	455.1	482.7	472	477.9	479.6
20%	427.1	423.9	426.3	426.3	431.8	424.8	463.5	410.4	471.7
25%	310	306.6	308	306.2	314.2	304.2	347.6	304.5	369.8
30%	202.2	201.3	205.3	200.7	214.3	201.3	226.3	201.9	237.9
40%	107.4	106.7	112.4	106.4	122.4	107.7	122.6	103.3	126.4
50%	47.7	47.5	52.5	48.6	62.7	48.2	57	48.2	63.2
Case 2	81W0	81C5	81C5(n.w.i.)	81C10	81C10(n.w.i.)	81C5T5	81C5T5(n.w.i.)	81C7T7	81C7T7(n.w.i.)
15%	513.2	513	510.8	518.2	505.1	518.5	523.9	515.1	544.1
20%	455.1	458.1	456	460.8	461.1	459.1	482.8	469.7	488.8
25%	329.6	328.8	329.1	331.6	332.4	334.5	358.5	335	371.9
30%	224.7	224.1	227.2	224.3	235.8	227.7	248.6	228.5	260.1
40%	125.4	125	129.6	124.9	139.7	126.8	142.2	128.1	144.6
50%	67.7	67.6	72.6	68.2	83.3	68.6	78.4	69.2	83.1
Case 3	81W0	81C5	81C5(n.w.i.)	81C10	81C10(n.w.i.)	81C5T5	81C5T5(n.w.i.)	81C7T7	81C7T7(n.w.i.)
15%	705.1	705.2	705.5	705.7	709.5	700.1	699.1	697.1	708.5
20%	517.1	514.2	519.3	508.9	524.2	511	528.3	506.1	527.3
25%	334.9	332	336.8	334.4	343.7	332.1	353.9	331.4	374.4
30%	206.8	204.8	212	204.5	224.3	198.7	220.8	198.4	232.6
40%	120.3	121.5	123	122.6	133.2	121.4	130.6	101.2	119.5
50%	64.1	64.1	68.4	61	75.6	63.1	68.9	63.4	71.9
Case 4	81W0	81C5	81C5(n.w.i.)	81C10	81C10(n.w.i.)	81C5T5	81C5T5(n.w.i.)	81C7T7	81C7T7(n.w.i.)
15%	472.5	471.7	476.7	463.8	483	472.9	494.4	473.7	495.3
20%	331.6	329.7	333.5	330.7	341.6	333.8	350.3	311.6	372.7
25%	212.1	211.5	212.4	210.8	224.6	213.4	248.5	214	265
30%	137	138.2	140.7	136.4	152.8	138.1	162.9	138.8	173.1
40%	71.8	72.1	76	71.1	87.1	71.3	85.7	67.4	87.9
50%	34.8	34.9	38.3	35.2	47.9	34.3	42.9	34.2	46.5

deviations of the IPP clouds (n.w.i.) are. When both the cross wind and the range (tail) wind were present, the wind-induced drift of the IPP clouds (n.w.i.) is compounded: without accounting for the cross wind, the IPP cloud (n.w.i.) deviates to one side (the right side in the cases discussed) of the major axis of the uncertainty ellipses (obtained by properly accounting for the wind effect in the dynamic model) while the lack of accounting for the tail wind causes the IPP cloud (n.w.i.) to be "pushed backward" causing range under-prediction.

6.3 Consistency Evaluation

The consistency of the MIMM estimator is very important in the IPP application. The consistency test will help to find the process noise setting that gives uncertainty ellipses compatible with the actual errors [1]. The

Table 6: IPP RMS errors (in m, 100 MC runs) for different OTs and different sensor accuracies, caliber 120 mm

Case 1	120W0	120C5	120C5(n.w.i.)	120C10	120C10(n.w.i.)	120C5T5	120C5T5(n.w.i.)	120C7T7	120C7T7(n.w.i.)
15%	748.3	745.7	740.6	753.3	742.3	742.8	769.5	728.9	794.9
20%	523.3	514.9	524	511.1	539.5	531.5	561.7	520.4	575.9
25%	431.1	427.1	435.2	420.5	440.4	436	433.7	451.5	450.8
30%	308.7	307.9	309.8	307.2	317.7	315.1	335.4	315.9	331.8
40%	130.9	130.9	134.2	131.1	142.2	132.6	144.9	128.8	150.2
50%	48.7	49.7	51.7	50.6	59.3	50.1	55.7	47.2	56.4
Case 2	120W0	120C5	120C5(n.w.i.)	120C10	120C10(n.w.i.)	120C5T5	120C5T5(n.w.i.)	120C7T7	120C7T7(n.w.i.)
15%	780.4	771.9	778	778	777.5	777.4	793.1	777.3	805.2
20%	611.4	611.1	610.5	604.8	613.3	604.1	620.5	610.5	633.3
25%	481.5	484.6	486.6	476.6	491.5	478	475.6	464.3	471.7
30%	349.9	354.3	355.4	353.1	361	349.5	361.7	349.6	377.3
40%	169.5	168.8	170.8	168.4	181.4	171.1	181.6	167.3	185.7
50%	66.1	66.7	69	67.4	77.5	67.4	72.9	63.1	75
Case 3	120W0	120C5	120C5(n.w.i.)	120C10	120C10(n.w.i.)	120C5T5	120C5T5(n.w.i.)	120C7T7	120C7T7(n.w.i.)
15%	914.3	919.4	914.5	936.6	916.7	897.8	938.6	906.3	948.4
20%	632.5	641.8	625.5	639.5	636.9	623.5	652	619.7	670
25%	426.2	414.7	422.4	414.5	418.5	418.8	443.9	386.5	430.2
30%	294.4	289.4	297.4	286.7	297.1	284.9	300	292	302.9
40%	143.4	140.1	146.8	143	156.5	141.9	151.8	141.5	150.9
50%	58.4	58.7	62.2	60.2	72.9	58.2	60.5	57.7	65
Case 4	120W0	120C5	120C5(n.w.i.)	120C10	120C10(n.w.i.)	120C5T5	120C5T5(n.w.i.)	120C7T7	120C7T7(n.w.i.)
15%	507.4	504.1	516.5	503.6	525.8	544	563	556.6	581.5
20%	490.8	497.6	500.5	496.8	514.3	518	453.3	526	475.1
25%	323.8	322.4	331.6	321	340	332.8	351	342.5	360.8
30%	194.5	195.1	199.4	194.1	208.3	210.2	218.5	211.6	231.6
40%	71.1	71	75.8	71.1	85.8	74.1	81.9	73.3	88.6
50%	35.2	34.9	37.4	34.7	44.9	36.7	38.5	33.1	40.7

consistency of the MIMM estimator is examined using both the normalized estimation error squared (NEES), which is preferable for Monte Carlo runs when the truth is available (off-line simulations), and the normalized innovation squared (NIS). The latter is the only one that can be used in real time testing [1].

Fig. 7 shows, for the best IMM estimator selected from the MIMM approach with OT=50% and different sensor accuracies, the NEES consistency in position and velocity and the NIS. Note that the NIS is evaluated for TM before the estimated BoP and for BM afterward [10]. It can be seen that as the sensor errors increase, the IMM estimator selected becomes less consistent. In particular, the larger the sensor's range error (which causes more uncertainty along the travel direction of the projectiles in present cases), the more significant is the inconsistency. Comparing the cases with smaller wind ("C5"/ "C5T5") to those (n.w.i.) and those with stronger wind ("C10"/"C7T7"), as the wind strength increases, the inconsistency of the IMM estimator becomes more significant in the later part of the observation window.

7. CONCLUSIONS

Using the MIMM approach developed in [10], the sensitivity of the IPP performance with respect to the total observation time, the wind effect and the sensor accuracy, are extensively studied. The total observation time is a critical factor for the IPP performance. Given the observation of the trajectory up to the apogee one can always expect a very good IPP performance; in many practical situations, the observation with OT=20% (given good sensor accuracies) is the minimum required to achieve an acceptable IPP performance with the IPP RMS error no more than 10% of the projectile range. The wind effect has significant influence on the IPP performance. The stronger the wind the greater is the IPP drift. The cross wind causes the IPP (n.w.i.) performance deviate to the side and the range (head/tail) wind causes the IPP (n.w.i.) to overshoot or undershoot the actual range of the projectile. The wind effect can be explicitly accounted for in the dynamic equation and fully compensated (with sufficient observation time) if the wind information is available. The sensor accuracy also has significant impact on the IPP performance. The sensor errors that cause more uncertainty along the travel direction of the projectiles are more crucial to IPP performance (in the present discussion, the range measurement error of the sensor has more impact on IPP performance than the angle measurement errors of the sensor).

Generally, to achieve the minimum acceptable IPP performance, i.e., that the IPP RMS error is within 10% of the projectile range, at least OT=15% (n.w.i) with the range measurement error up to 10 m and the angle errors up to 10 mrad are necessary. A condition to obtain good IPP performance is OT=20% (n.w.i) with the

range error less than 10 m and the angle errors less than 5 mrad. If the wind information is provided for the IPP procedure, both the total observation time and the sensor accuracy can be relaxed somewhat. There is a trade-off between the OT and the sensor accuracy, if the variations of both are in their reasonable regions (OT: $15\% \sim 30\%$; sensor range error: $5\,\text{m} \sim 25\,\text{m}$).

REFERENCES

[1] Y. Bar-Shalom, X. R. Li and T. Kirubarajan, *Estimation with Applications to Tracking and Navigation: Algorithms and Software for Information Extraction*, Wiley, 2001.

[2] Y. Bar-Shalom, P. K. Willett and X. Tian, *Tracking and Data Fusion*, YBS Publishing, 2011.

[3] X. R. Li and V. P. Jilkov, "Survey of Maneuvering Target Tracking. Part II: Motion Models of Ballistic and Space Targets", *IEEE Trans. Aerosp. Electronic Systems*, 46(1): 96-119, Feb. 2010.

[4] R. K. Mehra, "A Comparison of Several Nonlinear Filters for Reentry Vehicle Tracking", *IEEE Trans. Automatic Control*, AC-16(4): 307-319, Aug. 1971.

[5] R. W. Osborne, III, Y. Bar-Shalom and T. Kirubarajan, "Radar Measurement Noise Variance Estimation with Several Targets of Opportunity", *IEEE Trans. Aerosp. Electronic Systems*, 44(3): 985-995, July 2008.

[6] R. W. Osborne, III and Y. Bar-Shalom, "Statistical Efficiency of Composite Measurements from LoS Observation", *Proc. SPIE Conf. Signal Processing, Sensor Fusion and Target Recognition*, #8050-07, Orlando FL, April 2011.

[7] W. H. Press, B. P. Flannery, S. A. Teukolsky and W. T. Vetterling, *Numerical Recipes in FORTRAN: The Art of Scientific Computing, 2nd ed*, Cambridge University Press, 1992.

[8] V. Ravindra, Y. Bar-Shalom and P. K. Willett, "Projectile Identification and Impact Point Prediction", *IEEE Trans. Aerosp. Electronic Systems*, 46(4): 2004-2021, Oct. 2010.

[9] T. Yuan, Y. Bar-Shalom, P. K. Willett and D. Hardiman, "Impact Point Prediction for Short Range Thrusting Projectiles", *Proc. SPIE Conf. Signal and Data Processing of Small Targets*, #7698-55, Orlando FL, April 2010.

[10] T. Yuan, Y. Bar-Shalom, P. K. Willett, E. Mozeson, S. Pollak and D. Hardiman, "A Multiple IMM Estimation Approach with Unbiased Mixing for Thrusting Projectiles", *IEEE Trans. Aerosp. Electronic Systems*, accepted, 2011.

[11] US Army, "GTRAJ, General Trajectory Program, US Army (Version 6.21)".

[12] http://www.braeunig.us/space/cd.htm

[13] http://en.wikipedia.org/wiki/External_ballistics

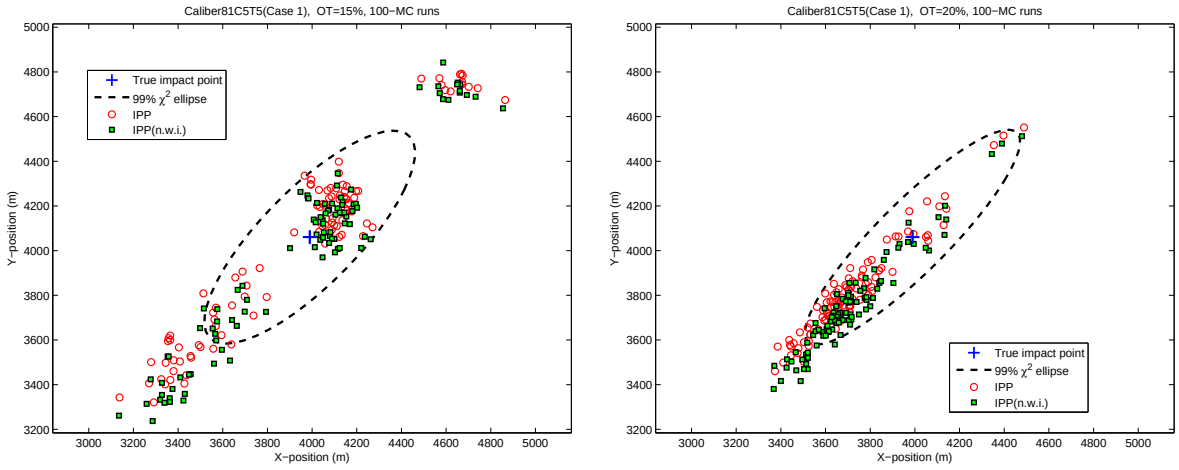

(a) OT=15%

(b) OT=20%

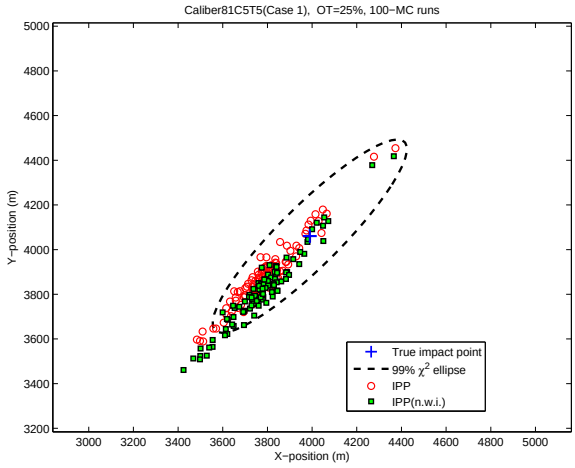

(c) OT=25%

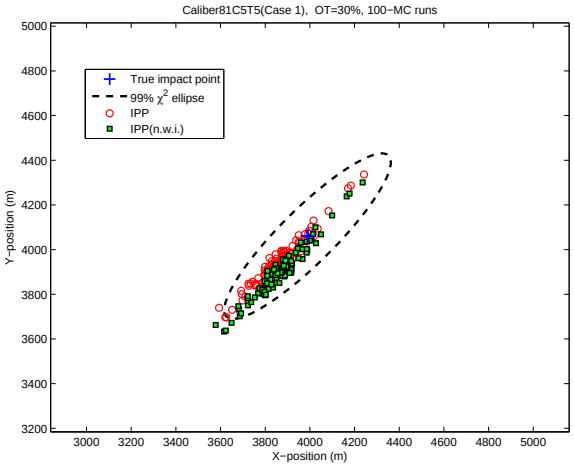

(d) OT=30%

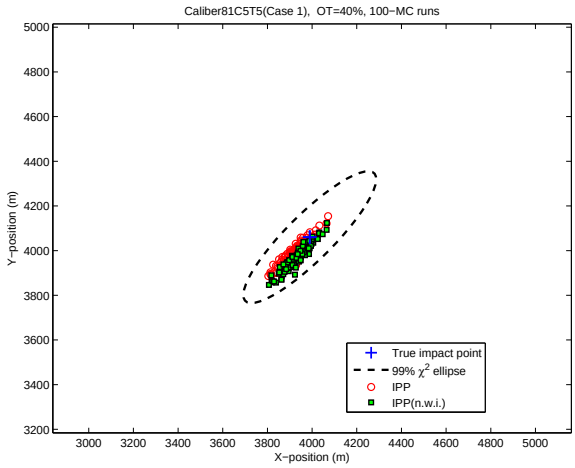

(e) OT=40%

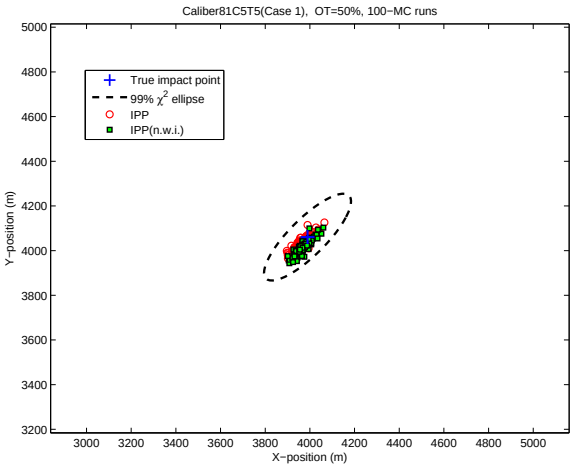

(f) OT=50%

Figure 4: The IPP uncertainty ellipse and MC IPP cloud for different OTs, trajectory 81C5T5, *Case* 1, 100 MC runs

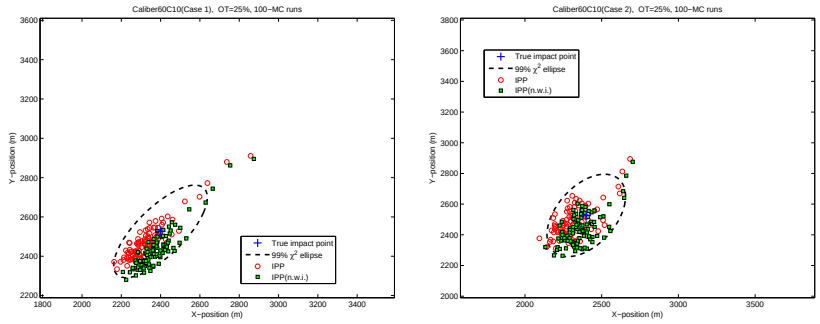

(a) *Case*-1 (b) *Case*-2

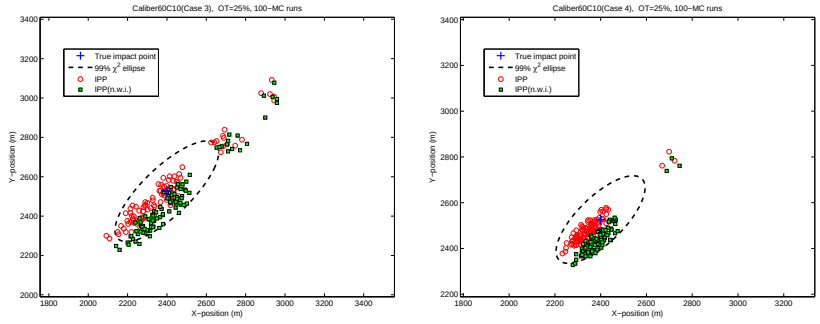

(c) *Case*-3 (d) *Case*-4

Figure 5: The IPP uncertainty ellipse and MC IPP cloud for different sensor accuracies, trajectory 60C10, OT=25%, 100 MC runs

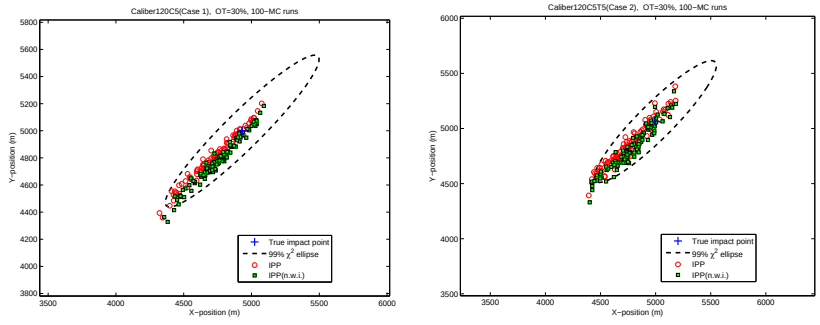

(a) Trajectory 120C5 (b) Trajectory 120C5T5

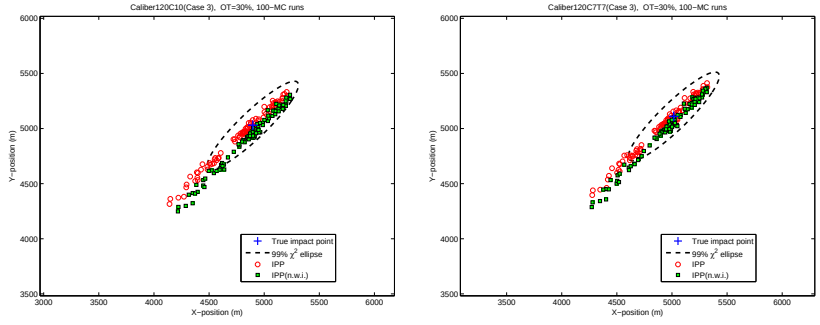

(c) Trajectory 120C10 (d) Trajectory 120C7T7

Figure 6: The IPP uncertainty ellipse and MC IPP cloud for different 120mm trajectories, OT=30% 100 MC runs

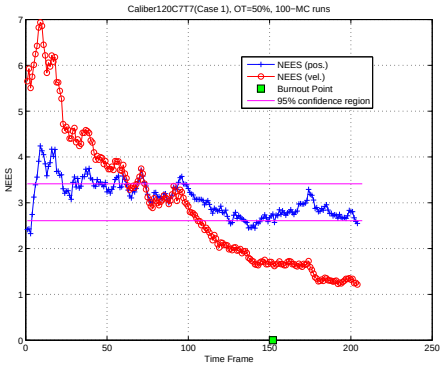

(a) NEES (pos. and vel.), g.w.i., *Case* 1

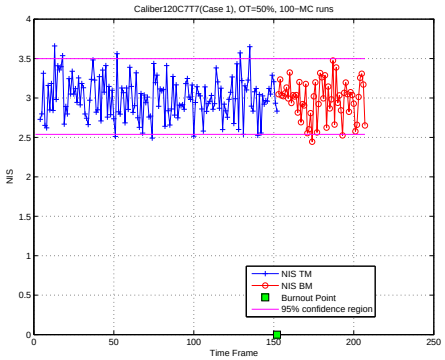

(b) NIS, g.w.i., *Case* 1

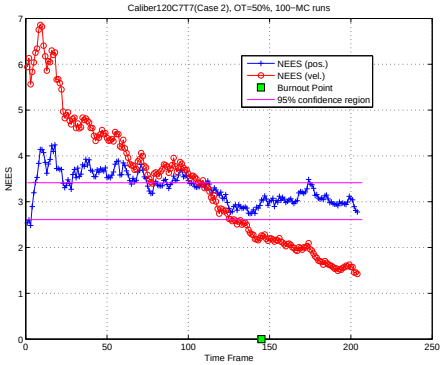

(c) NEES (pos. and vel.), g.w.i., *Case* 2

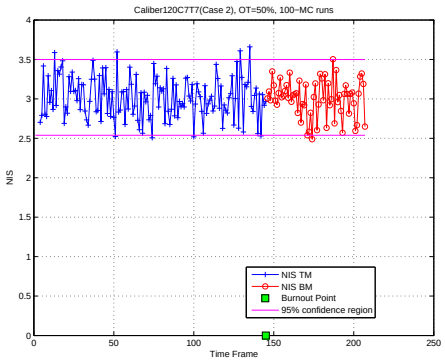

(d) NIS, g.w.i., *Case* 2

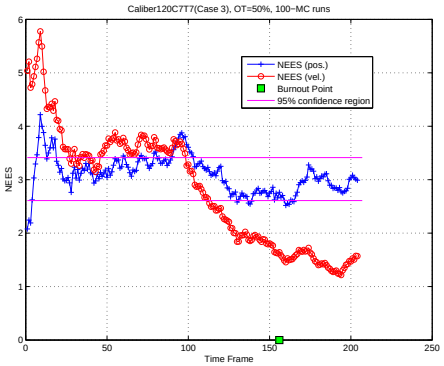

(e) NEES (pos. and vel.), g.w.i., *Case* 3

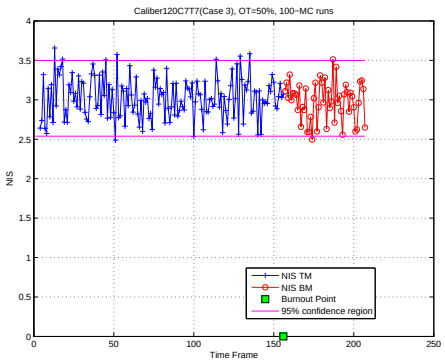

(f) NIS, g.w.i., *Case* 3

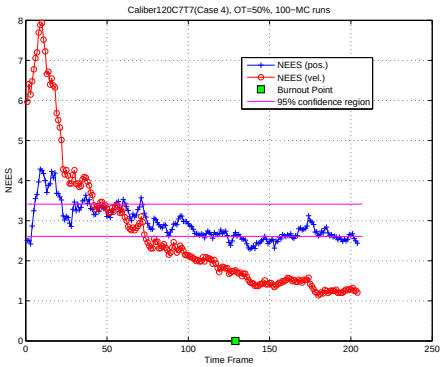

(g) NEES (pos. and vel.), g.w.i., *Case* 4

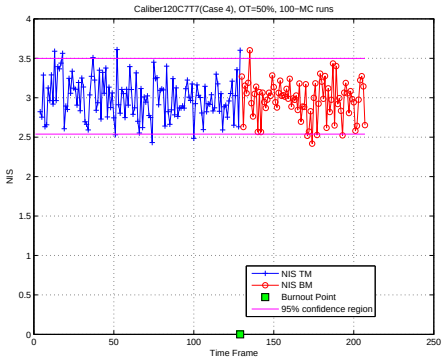

(h) NIS, g.w.i., *Case* 4

Figure 7: Consistency test (NEES in pos. and vel. and NIS), trajectory 120C7T7, OT=50%, 100-MC run